Contactless Breathing Rate Monitoring in Vehicle Using UWB Radar

Zhicheng Yang
University of California, Davis, CA, USA
zcyang@ucdavis.edu

Maurizio Bocca
Bosch RTC, Sunnyvale, CA, USA
Maurizio.Bocca@us.bosch.com

Vivek Jain
Bosch RTC, Sunnyvale, CA, USA
Vivek.Jain@us.bosch.com

Prasant Mohapatra
University of California, Davis, CA, USA
pmohapatra@ucdavis.edu

ABSTRACT

Monitoring human vital signs is fundamental to assess a person's general health and detect events such as respiratory distress or heart attacks. As vehicle driving occupies a considerable part of daily lives, monitoring vital signs of a driver is necessary for early detecting potential health issues during driving. However, it is also important to ensure that the driver is neither distracted nor uncomfortable while monitoring. It is thus a challenge to develop contactless and ubiquitous vital sign monitoring. This paper presents contactless breathing rate monitoring for drivers using an impulse ultra-wide band (UWB) radar. We demonstrate that UWB frequency reflects signals from human body and validate a UWB radar for detecting the minute chest movement. Two signal processing methods are designed and evaluated for on-line and off-line analysis. We investigate 16 different radar positions in a vehicle for robust breathing rate monitoring under the circumstance of body motions during driving. We also perform on-road experiments at a local city and achieve a mean of 1.06 breathing rate estimation error per minute.

CCS CONCEPTS

• **Human-centered computing → Ubiquitous and mobile computing**;

KEYWORDS

Breathing rate, Healthcare, Ultra-wide band, Smart driving

ACM Reference Format:
Zhicheng Yang, Maurizio Bocca, Vivek Jain, and Prasant Mohapatra. 2018. Contactless Breathing Rate Monitoring in Vehicle Using UWB Radar. In *7th International Workshop on Real-World Embedded Wireless Systems and Networks (RealWSN'18), November 4, 2018, Shenzhen, China.* ACM, New York, NY, USA, 6 pages. https://doi.org/10.1145/3277883.3277884

1 INTRODUCTION

Monitoring vital signs such as breathing rate can offer crucial insights for human's well-being and indicate a wide range of medical problems. However, continuous monitoring of a person's vital signs is a challenging problem. Current solutions require the person to wear some dedicated smart wristband, chest straps, or compression garment. Such wearable devices are required to attach to the human's body all the time, making them less convenient. This has motivated the design of contactless solutions for vital sign monitoring where ambient wireless signals can be leveraged for the purpose. Meanwhile, as the time people spend on driving contribute to an inevitable part of a whole day now, monitoring vital signs of a driver will enable early detection of health issues or drowsy fatigue during driving which can improve road safety.

This paper presents our current progress of vital sign monitoring in vehicle using ultra-wide band (UWB) frequency, especially with the focus of breathing rate monitoring for a driver. UWB has been used for various sensing applications for decades. Compared to other frequency bands, UWB is less affected by multipath propagation effects, achieving high sensing resolution and precision. This frequency band also has the additional advantage of complexity of system design [8]. These merits enable to deploy such radar sensors in vehicles at a very low cost. Vital sign monitoring is an important application for UWB sensing [4, 11, 14]. Most of these solutions focus on office or home environment. However, monitoring vital signs in vehicle is non-trivial. Unlike the still indoor environment, a powered-on vehicle has its engine vibrations, which introduces additional passive minute body movements. Furthermore, frequent and unpredictable body motions caused by driving habits, or by operating the steering wheel and the control panel, etc., keep occurring during driving. Since space in vehicle is very limited, such body motions sensitively impact the signal propagation very much, and further downgrade the estimation performance. In this paper, we demonstrate that UWB signals bouncing off a human body can sensitively detect the minute chest movement necessary to accurately estimate a human's breathing rate at the driver's seat during driving. Our contributions can be summarized as follows:

(1) We study the reflection coefficient of human skin under UWB frequency to formalize the feasibility of UWB signal reflected off human body.
(2) The breathing rate estimation at an expected radar position should be robust to the interference of regular driving motions. We investigate the UWB radar placements at 16 different positions in a vehicle, and suggest the position of rear view mirror to achieve a confident breathing rate estimation.
(3) All of in-vehicle experiments are done in powered-on vehicles. Hence, our evaluation results have included the condition of vehicle vibrations. Our results show that the breathing rate estimation of our system is robust to vehicle vibrations.
(4) We present and evaluate two signal processing methods for off-line or on-line analysis.

RealWSN'18, November 4, 2018, Shenzhen, China

ACM ISBN 978-1-4503-6048-7/18/11…$15.00
https://doi.org/10.1145/3277883.3277884

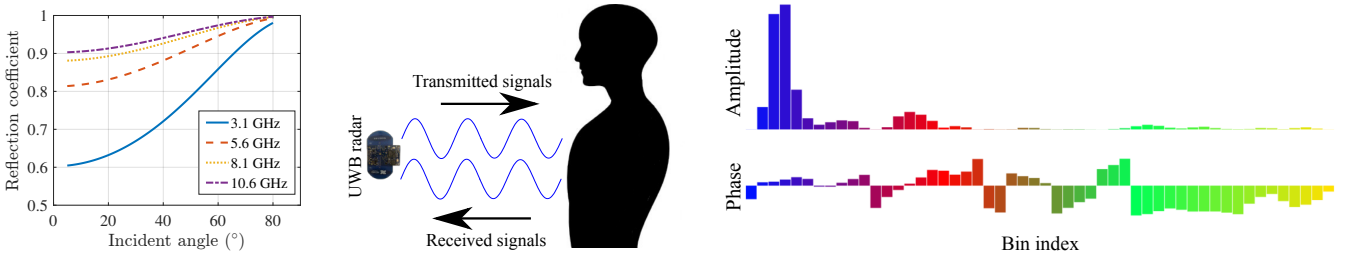

(a) Reflection coefficients of 1mm human skin with its relative permittivity of 40

(b) Detection of chest movement using a UWB radar

(c) Example display of range bins of X2M200 radar. Gradual changes in colors are only for differentiating range bins

Figure 1: Reflection coefficients and UWB radar sensing

The paper is organized as follows. The feasibility of detecting chest movement using UWB is discussed in Sec. 2. UWB radar placement and signal processing methods are provided in Sec. 3. We evaluate the breathing rate estimation in vehicles in Sec. 4. Future works are listed in Sec. 5. Related works are discussed in Sec. 6. We conclude in Sec. 7.

2 FEASIBILITY OF USING UWB RADAR TO MONITOR BREATHING RATE

In this section, we investigate the feasibility of using UWB frequency to detect a human's chest movement. First we study the signal reflection propagation onto a human body, then validate the radar device we use for the breathing detection.

2.1 UWB signal reflection on human skin

We first investigate the UWB signal reflection on human skin. The amount of signals reflected from an object can be quantified using *reflection coefficient*. The reflection coefficient (r) can be used to estimate the power loss due to reflection (or power reflection coefficient) as $R = \frac{P_O}{P_I} = |r|^2$ where P_O and P_I are the values of reflected (after reflection) and incident (before reflection) power, respectively. The reflection coefficient (r) is calculated [3] as

$$r = \frac{1 - e^{-j2\omega}}{1 - r_i^2\, e^{-j2\omega}}\, r_i, \qquad \text{for } i \in \{\perp, \parallel\} \tag{1}$$

where $\omega = \frac{2\pi l}{\lambda}\sqrt{\epsilon_2/\epsilon_1 - \sin^2\gamma}$, l refers to the thickness of the reflecting source; λ denotes the signal wavelength; γ is the incident angle; ϵ_1 and ϵ_2 are the permittivities of the first medium and the second medium, respectively. In a simplified single layer model, the first medium can be assumed as air which has the permittivity of 1. $r_\perp$ and $r_\parallel$ are the Fresnel's reflection coefficients when the electric field is perpendicular and parallel to the incidence plane, respectively. The $r_\perp$ is calculated as

$$r_\perp = \frac{\cos\gamma - \sqrt{\epsilon_2/\epsilon_1 - \sin^2\gamma}}{\cos\gamma + \sqrt{\epsilon_2/\epsilon_1 - \sin^2\gamma}}. \tag{2}$$

We calculate the reflection coefficient of human skin using the Eq. 1 and 2 with perpendicular waves. The results of 1-mm human skin with its relative permittivity of 40 [28] are shown in Fig. 1a. Under the FCC regulation, UWB for medical usages is limited to 3.1 – 10.6 GHz [17]. As we can see, the reflection coefficients of the medical UWB range are larger than 0.6 at various incident angles. When the operating frequency is higher, the reflection coefficient monotonically increases.

2.2 Radar range bins

We select a low-cost Xethru X2M200 impulse UWB radar [16] for our breathing rate measurements, as it can provide mm-level resolution [24]. The operation of X2M200 is to *bin* the received signals, which means that the received signals contribute a sorted set of bins by ToA of transmitting pulses. The time interval is proportionally determined by the radar signal round-trip distance created by the reflection from the object. Radar is then able to know the object's distance to the transceiver based on the signal arrivals across the different bins [13]. Fig. 1c shows an example display of range bins provided by Xethru X2M200. It has 52 normalized amplitude bins and 52 radian phase bins. The length between each bin is 3.84cm [16]. The monitoring range (0.5 – 2.5m) is covered by the bins (from left to right).

It is worth noting that Xethru has its own software to display one's breathing effort. However, there are two limitations: 1) the raw amplitude and phase data are not available via its software interface; 2) when a monitored subject performs body motions, the software will simply interrupt the display but present the notification of "subject has body motions" only. As our objective is to continuously monitor the breathing rate in a non-stationary environment, we program our scripts to access Xethru's API and to acquire the raw amplitude and phase data at a sampling rate of 20 Hz.

2.3 Chest movement detection

In Fig. 1c, the amplitudes at the first four bins rise high. This is because we place the radar in front of a subject at a distance of around 0.6m (illustrated in Fig. 1b) to verify the radar performance of chest movement detection. Fig. 3a shows the signal amplitude at one example range bin (from Fig. 1c) during the subject's existence, where breathing patterns are clearly found (~19 breathings). The corresponding frequency domain information using the fast Fourier transform algorithm (FFT) is shown in Fig. 3b. We observe that the UWB signals are very sensitive to periodic movements of human breathing.

3 BREATHING RATE MONITORING IN VEHICLE ENVIRONMENT

3.1 Radar placements

Compared to breathing rate monitoring in common living spaces, the space in vehicles is limited. A person's body motions will sensitively impact the signal propagation, leading to the amplitude and phase changes. Fig. 2 presents the amplitude and phase variations of one subject sitting at the driver's seat over 2 minutes at

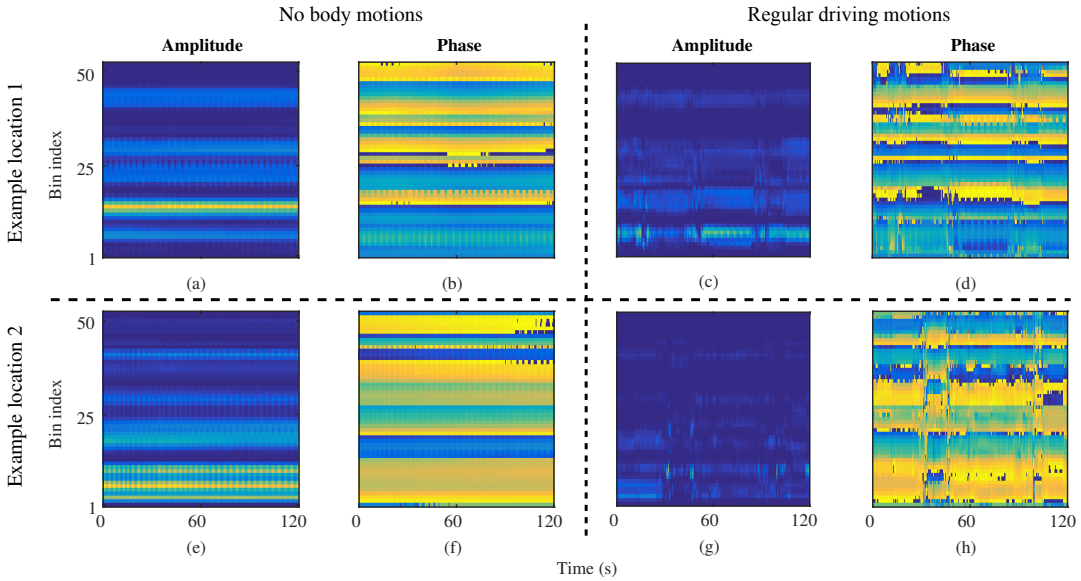

Figure 2: Performances of some example positions for radar placements

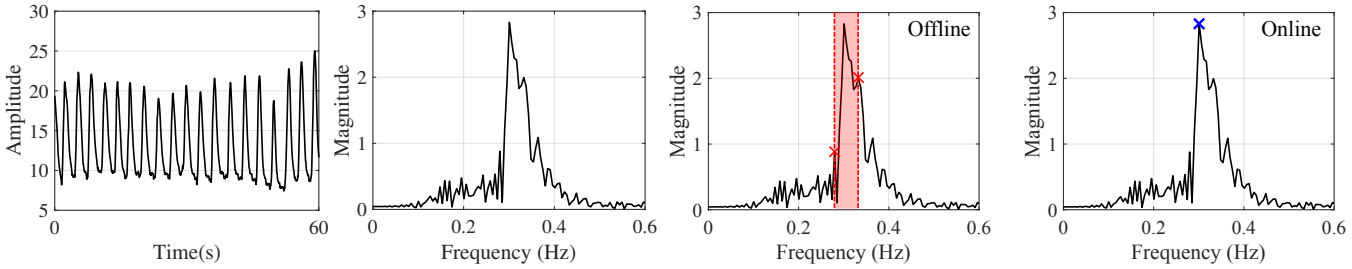

(a) Example amplitude to indicate the breathing patterns

(b) FFT of Fig. 3a

(c) Off-line method

(d) On-line method

Figure 3: Signal processing example

2 example positions of the UWB radar. As we can see, when the subject has no body motions (sitting still at the seat and normally breathing only), the amplitude and phase data of both two positions have obvious periodic variations ((a), (b); (e), (f)). However, when the subject performs some body motions during driving, such as turning the steering wheel around, operating the control panel, turning the head, adjust the seating position, etc., the amplitude and phase data is much noisy at Example position 2 ((g), (h)). The periodic variations are very difficult to be identified. Instead, Example position 1 ((c), (d)) keeps the hint of periodic patterns on the amplitude and phase data. Although Position 1 is supposed to have the better performance, it is still quite challenging to estimate the breathing rate purely depending on such noisy time-series data.

3.2 Signal processing

In order to better estimate the breathing rate, we transform the amplitude and phase data to the frequency domain (Fig. 3a and 3b). We present one off-line and one on-line signal processing methods for breathing rate estimation, and evaluate them in Sec. 4.2.

Off-line method. The sensitivity of amplitude and phase signals to periodic chest movements results in a peak (dominant frequency) in the frequency domain. However, the corresponding frequency of this peak estimates the breathing rate in each range bin at a coarse-grain level. Instead, we select the two adjacent peaks of the highest peak [2] (shown in Fig. 3c), and create a custom narrow band-pass filter. We calculate the mean boundary values over all 104 bins (52 amplitude + 52 phase in Fig. 1c). This custom filter is then applied on the amplitude and phase data, and a simple peak detection algorithm is used for estimating the breathing rate in Bpm (breathing per minute).

On-line method. A moving sliding window is applied on the measured data to enable the real-time breathing rate monitoring of a subject. Instead of creating a custom filter in the off-line method, the estimated breathing rate in Bpm is achieved by multiplying the highest magnitude peak at the frequency domain in a sliding window, with 60 seconds (shown in Fig. 3d). Since the moving sliding window is able to involve with the newest data input stream, even though a simple multiplication is performed in every sliding window, the average estimation error across the time flow can be mitigated. Meanwhile, the size of sliding window is an important factor to impact the performance.

4 EVALUATION

In this section, we first evaluate various radar positions in a real vehicle. One selected radar position is then used for further evaluations. We use a Xethru X2M200 radar to collect the breathing data, and a USB pressing button to obtain the ground truth of breathing counts. The button is pressed while a subject is inhaling. Both data

Figure 4: Equipment setup for the experiments

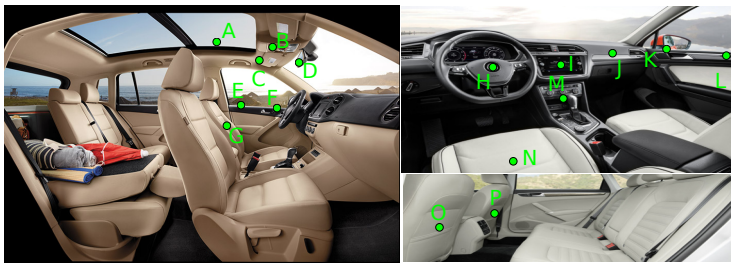

Figure 5: 16 actual positions of radar placement in a vehicle

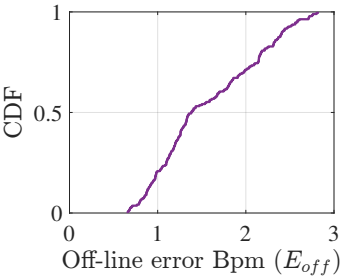

Figure 6: CDF of off-line error Bpm (E_{off}) of all radar placement experiments

Segment of $\bar{E}_{off}$	$\bar{E}_{off} \leq 1$	$1 < \bar{E}_{off} \leq 2$	$\bar{E}_{off} > 2$
Representative position	Position D	Position C	Position E
	Position O	Position H	Position I

Table 1: Average estimation error ($\bar{E}_{off}$) of breathing rate at different radar positions when the driver subjects perform regular body motions during driving

streams are time-aligned into a laptop host (shown in Fig. 4). We keep the vehicle powered-on for all the experiments to involve the vehicle vibrations. Except from the on-road tests, the vehicle is parked for the other experiments. There are 4 driver participants (3 males and 1 female) in our experiments. The range of their ages spans from 29 to 55 years old, while the body mass index (BMI) is from 20.7 to 28.3.

4.1 Radar placements

We test 16 different radar positions around the driver's seat. Fig. 5 depicts the actual placement positions (Position A to P). We collect 2-minute breathing data from subjects at the driver's seat, while they emulate regular driving behaviors (performing some regular body motions during driving as aforementioned in Sec. 3). The off-line signal processing method is applied in this radar placement evaluation. The experiment at each position is repeated for 3 times.

For better presenting and evaluating the performance, we leverage the common used metric *error Bpm* to evaluate the quality of breathing rate estimation, which refers to the absolute difference between the estimated Bpm and the ground truth Bpm. We let E_{off} denote the off-line error Bpm. Fig. 6 presents that the cumulative distribution of all E_{off} results of 192 experiments (16 radar positions × 4 subjects × 3 times). We calculate the average off-line error Bpm ($\bar{E}_{off}$) of each radar position. All $\bar{E}_{off}$ results are then divided into three sections: $\bar{E}_{off} \leq 1$, $1 < \bar{E}_{off} \leq 2$, and $\bar{E}_{off} > 2$. Table 1 presents the segmented estimation results. As we can see, one of the best positions in our experiment is the rear view mirror (Position D). This position is able to create a relative Line-of-Sight (LoS) round-way sensing propagation to achieve a confident breathing rate estimation ($\bar{E}_{off} \leq 1$). It is interesting that the position of the back of driver's seat (Position O) also has a great performance. Regardless of the seat itself between driver's back and the radar, the signal is still able to penetrate the fabrics and bounce off the driver's back at the UWB frequency. Furthermore, this position is unlikely interfered by arm motions. The center of steering wheel (Position H) is a common position in other literature [9], however, its performance in our experiment is not as good as that of Position D. The very short distance between the center of steering wheel and the driver's chest might slightly introduce some arm motions as false positives. The position of above the handle of driver's side door (Position E) and the position of central panel (Position I) severely suffer from the arm motion effects, which frequently interfere the signal propagation path to/from chest movements. Based on the performance and convenience of deployment, we select Position D as the radar placement position in the following evaluations.

4.2 Knowledge of sliding window

We next investigate the appropriate size of sliding window as it is an important factor of the signal processing procedure. We design three breathing scenarios: 1) normal breathing without body motions in vehicles; 2) normal breathing with regular driving motions; 3) a mixture of normal, fast and slow breathings with regular driving motions. We fix the moving speed of sliding window as 1 second, i.e. the updating frequency of breathing rate estimation is 1 Hz. Each of the experiments is measured for 10 minutes.

We process the breathing data by using the on-line signal processing method (with sliding window) and the off-line method (without sliding window) for each scenario. The size of 2-second to 40-second sliding windows are tested. We here let E_{on} denote the on-line error Bpm at every updating time of 1 Hz, and calculate the average on-line error Bpm ($\bar{E}_{on}$) across the timeline. The results of $\bar{E}_{on}$ and $\bar{E}_{off}$ are shown in Fig. 7. Even though all of $\bar{E}_{on}$ have some jitters at the very beginning, as the sliding window size increases, they gradually go down. It is natural that the scenario of normal breathing and no body motions has the best overall performance (Fig. 7a), where the advantage of sliding window is not obvious. When the body motions are introduced in Fig. 7b, the $\bar{E}_{on}$ is always lower than $\bar{E}_{off}$. Furthermore, when subjects intentionally vary the breathing frequency to emulate some breathing symptom during driving. The on-line method with the usage of sliding window outperforms the off-line method very much (shown in Fig. 7c). Based on the results we observe that when the size of sliding window is larger than 10-second, the $\bar{E}_{on}$ tends to be stable and the system achieves a robust breathing rate estimation. Fig. 8 shows that the cumulative distribution of all of E_{on} for three different breathing combinations using a sliding window size with the size of 30-second. The combination of varying breathings and body motions has much larger variation of estimation errors.

4.3 On-road breathing rate estimation

We do our on-road tests on the local streets at Davis, CA, using three vehicles, Volkswagen Tiguan 2015, Volkswagen Jetta 2016,

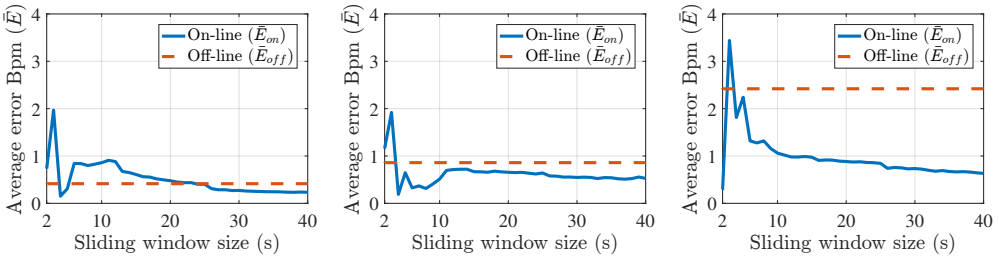

(a) Average estimation error of breathing rate for normal breathing without body motions

(b) Average estimation error of breathing rate for normal breathing with regular driving motions

(c) Average estimation error of breathing rate for mixed normal, fast, and slow breathings with regular driving motions

Figure 7: Average estimation error of breathing rate for different combinations of various breathing behaviors and body motions

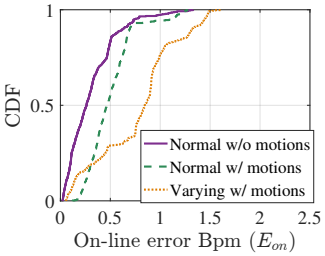

Figure 8: CDF of on-line error Bpm (E_{on}) of three breathing combinations. "Normal" refers to normal breathing; "Varying" refers to mixture of normal, fast, and slow breathings

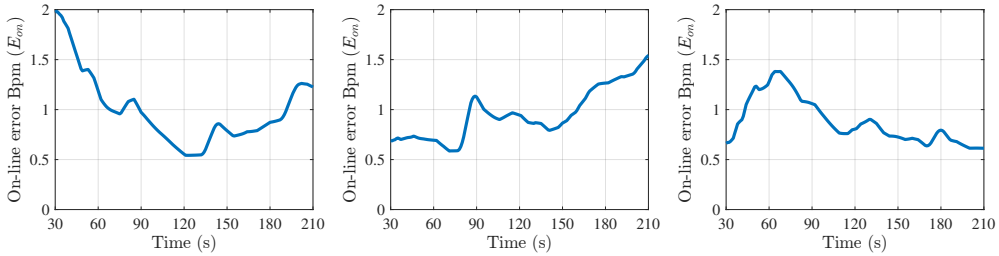

(a) Estimation error of breathing rate for Example route 1

(b) Estimation error of breathing rate for Example route 2

(c) Estimation error of breathing rate for Example route 3

Figure 9: Example of breathing rate estimation error (E_{on}) over time for three routes created by one subject

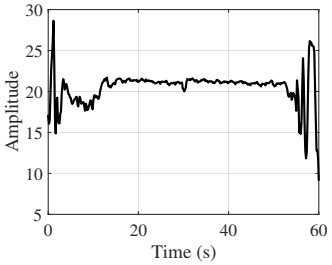

Figure 10: Example of subtle chest movement detection when a holds her breathing subject

and Toyota Corolla 2010. The speed limitation range of the driving tests spans 15 – 45 mph, including parking lot driving (~15 mph), local driving (~30 mph), and local speedway driving (~45 mph). The driving routes depend on where the subject wants to visit. Each subject follows his/her own driving habits and routes, and performs the ~4-minute driving for 3 times (totally ~12-minute driving). Apart from a subject's active body motions, the passive body movements caused by unexpected various bumps or dips on roads make the breathing rate estimation more challenging. Hence, we apply a 30-second sliding window size for stability.

Fig. 9 depicts the on-line error Bpm (E_{on}) changes along with the time for three example routes created by a subject. In Fig. 9a, the beginning one minute suffers from large E_{on} while the subject repeats driving on a circle route in a community. The periodical behavior of turning steering wheel interferes with the frequency peak of breathings. The similar observation is found at the last two minutes in Fig. 9b, while the subject is performing multiple U-turn driving. In Fig. 9c, the last 2 minutes have a small E_{on} while the subject is driving on a ~2-mile long local speedway with smooth traffic.

Overall, the average error Bpms of all subjects are 0.86, 1.07, 1.02, 1.30, respectively. Compared to other literature [10], our results are within the acceptable range. The larger estimation error of Subject 4 may be caused by his relatively lower height, leading to a misalignment of radar sensing direction (at Position D) and his chest height, and by a higher BMI value, which is correlated with the breathing rate [22].

5 DISCUSSION, FUTURE WORKS, AND POTENTIALS

We notice that the on-line method outperforms the off-line method which makes us believe that sliding window method adapts better than bandpass filter method when there is variability in breathing rate of the driver. The awareness of pressing the button to count the breathings is also a possible factor of distraction. These observations motivate us to refine the methods of off-line breathing rate estimation, of the ground truth acquisition, and the driving test in various specific scenarios and behaviors in our future work to clarify the cases where UWB radar monitoring perform better or worse. Moreover, clothing type is also a valuable aspect to be studied, as different clothing materials are potential to change the reflectivity.

Although the UWB radar we use claims itself as a radar for breathing monitoring only [16], we do notice the minute periodical vibrations corresponding to the heart beats across the range bins when subjects hold the breaths. An example when a subject holds her breath is shown in Fig. 10. Heart rate along with breathing rate monitoring is thus our ongoing target. We will also involve some various highway road tests, including jammed and smooth highway sections, because traffic obstructions may annoy drivers and then influence their vital signs [6]. Concurrently monitoring vital signs of multiple persons in vehicles will be also investigated.

Our proposed system is not limited within one individual vehicle. Instead, its flexibility is able to construct a connected health system in the Internet of Vehicles (IoV). With the emerging era of edge cloud computing in the Internet of Things [23], it enables to

comprehensively monitor drivers' health conditions in real time and ultimately improve the overall safety of driving in IoV.

6 RELATED WORKS

6.1 Vital sign monitoring using UWB radar

UWB radar is used for medical applications for decades [17]. Authors in [14] demonstrated the high correlation between chest movement detection using UWB frequency and respiratory chest belt. Vital sign monitoring using UWB frequency was also validated [11]. Additionally, authors in [4] demonstrated the capability of using UWB radar to sense human's vital signs through a wall. Those studies mainly focus on indoor still scenarios. An impulse UWB radar testbed for vital sign monitoring was designed in [20]. Their focus was to monitor infant or child sleeping health in vehicle during the hot weather, while our objective is to monitor driver's vital sign for safe driving. Authors in [10] studied using UWB radar to monitor driver's vital sign and mobile phone usage. However, the radar placement was not investigated, and on-road tests were not fully covered. Vital sign monitoring for different subject's orientations with a movement compensation method was presented by [24]. In our case, a subject is supposed to always face the front.

6.2 Vital sign monitoring using other wireless technologies

Fine-grained Channel State Information (CSI) of WiFi was leveraged to monitor vital signs [2, 12]. The primary focus of the work to measure the vital signs when a person is sitting or sleeping in a stable environment. The authors in [1] proposed to use WiFi RSS for respiratory monitoring. However, it requires the person to hold a device or stand in the line-of-sight path between TX and RX nodes for accurate monitoring. 60 GHz millimeter wave is regarded as an upcoming technology for the next generation of WiFi with the IEEE 802.11ad standard [15, 25, 27]. Authors in [5, 26] validated the feasibility of 60 GHz mmWave signals for vital sign monitoring under different facing orientations. These systems are primarily designed for indoor living scenarios. Wireless Sensor Networks (WSNs) were deployed in hospital wards for vital sign monitoring [7]. Authors in [19] presented a WSN system using 802.15.4 devices to monitor vital signs. Such systems require the deployment of plentiful sensor nodes and advanced routing protocols [21] for accurate monitoring without much time delay, and might have potential security issues [18].

7 CONCLUSION

In this paper, we present a contactless breathing rate monitoring system in vehicles utilizing impulse UWB signals reflected from human body. The capacity of UWB frequency to detect the minute chest movement is demonstrated. We investigate the radar placement among 16 different radar positions in a powered-on vehicle for robust breathing rate monitoring, and find the rear view mirror is a confident position. We also evaluate four participants for on-road experiments and achieve a mean of 1.06 breathing rate estimation error per minute.

REFERENCES

[1] Heba Abdelnasser, Khaled A Harras, and Moustafa Youssef. 2015. UbiBreathe: A ubiquitous non-invasive WiFi-based breathing estimator. In *ACM MobiHoc 2015.*

[2] Fadel Adib, Hongzi Mao, Zachary Kabelac, Dina Katabi, and Robert C Miller. 2015. Smart homes that monitor breathing and heart rate. In *Proceedings of the 33rd annual ACM conference on human factors in computing systems.* ACM, 837–846.

[3] Javad Ahmadi-Shokouh, Sima Noghanian, Ekram Hossain, Majid Ostadrahimi, and James Dietrich. 2009. Reflection coefficient measurement for house flooring materials at 57-64 GHz. In *IEEE Globecom.*

[4] MYW Chia, SW Leong, CK Sim, and KM Chan. 2005. Through-wall UWB radar operating within FCC's mask for sensing heart beat and breathing rate. In *IEEE European Radar Conference (EURAD) 2005.*

[5] Huey-Ru Chuang, Hsin-Chih Kuo, Fu-Ling Lin, Tzuen-Hsi Huang, Chi-Shin Kuo, and Ya-Wen Ou. 2012. 60-GHz millimeter-wave life detection system (MLDS) for noncontact human vital-signal monitoring. *IEEE Sensors Journal* (2012).

[6] Jerry L Deffenbacher, Eugene R Oetting, and Rebekah S Lynch. 1994. Development of a driving anger scale. *Psychological reports* (1994).

[7] Rahav Dor, Gregory Hackmann, Zhicheng Yang, Chenyang Lu, Yixin Chen, Marin Kollef, and Thomas Bailey. 2012. Experiences with an end-to-end wireless clinical monitoring system. In *Proceedings of the conference on Wireless Health.* ACM, 4.

[8] Igor I Immoreev and PGS Dmitry V Fedotov. 2002. Ultra wideband radar systems: advantages and disadvantages. In *IEEE Ultra Wideband Systems and Technologies, 2002.*

[9] Boon-Giin Lee and Wan-Young Chung. 2012. A smartphone-based driver safety monitoring system using data fusion. *Sensors* (2012).

[10] Seong Kyu Leem, Faheem Khan, and Sung Ho Cho. 2017. Vital Sign Monitoring and Mobile Phone Usage Detection Using IR-UWB Radar for Intended Use in Car Crash Prevention. *Sensors* 17, 6 (2017), 1240.

[11] Mario Leib, Wolfgang Menzel, Bernd Schleicher, and Hermann Schumacher. 2010. Vital signs monitoring with a UWB radar based on a correlation receiver. In *Antennas and Propagation (EuCAP), 2010 Proceedings of the Fourth European Conference on.* IEEE, 1–5.

[12] Jian Liu, Yan Wang, Yingying Chen, Jie Yang, Xu Chen, and Jerry Cheng. [n. d.]. Tracking vital signs during sleep leveraging off-the-shelf wifi. In *ACM MobiHoc 2015.*

[13] Bassem R Mahafza. 2005. *Radar Systems Analysis and Design Using MATLAB Second Edition.* Chapman and Hall/CRC.

[14] Yogesh Nijsure, Wee Peng Tay, Erry Gunawan, Fuxi Wen, Zhang Yang, Yong Liang Guan, and Ai Ping Chua. 2013. An impulse radio ultrawideband system for contactless noninvasive respiratory monitoring. *IEEE Transactions on Biomedical Engineering.*

[15] Thomas Nitsche, Carlos Cordeiro, Adriana B Flores, Edward W Knightly, Eldad Perahia, and Joerg C Widmer. 2014. IEEE 802.11 ad: directional 60 GHz communication for multi-Gigabit-per-second Wi-Fi. *IEEE Communications Magazine* 52, 12 (2014), 132–141.

[16] Novelda. 2015. X2M200. https://www.xethru.com/shop/x2m200-respiration-sensor.html.

[17] Jianli Pan. 2007. Medical applications of ultra-wideband (uwb). *Survey* (2007).

[18] Jianli Pan and Zhicheng Yang. 2018. Cybersecurity Challenges and Opportunities in the New Edge Computing+ IoT World. In *Proceedings of the 2018 ACM International Workshop on Security in Software Defined Networks & Network Function Virtualization.* ACM, 29–32.

[19] Neal Patwari, Lara Brewer, Quinn Tate, Ossi Kaltiokallio, and Maurizio Bocca. 2014. Breathfinding: A wireless network that monitors and locates breathing in a home. *IEEE Journal of Selected Topics in Signal Processing* 8, 1 (2014), 30–42.

[20] Bernd Schleicher, Ismail Nasr, Andreas Trasser, and Hermann Schumacher. 2013. IR-UWB radar demonstrator for ultra-fine movement detection and vital-sign monitoring. *IEEE transactions on microwave theory and techniques* 61, 5 (2013), 2076–2085.

[21] Junyang Shi, Mo Sha, and Zhicheng Yang. 2018. DiGS: Distributed Graph Routing and Scheduling for Industrial Wireless Sensor-Actuator Networks. In *IEEE ICDCS.*

[22] Molly Sorlien. 2017. BMI and Respiratory Function. https://www.livestrong.com/article/84685-bmi-respiratory-function/.

[23] Jianyu Wang, Jianli Pan, Flavio Esposito, Prasad Calyam, Zhicheng Yang, and Prasant Mohapatra. 2018. Edge Cloud Offloading Algorithms: Issues, Methods, and Perspectives. *arXiv preprint arXiv:1806.06191* (2018).

[24] Dag T Wisland, Kristian Granhaug, Jan Roar Pleym, Nikolaj Andersen, Stig Støa, and Håkon A Hjortland. 2016. Remote monitoring of vital signs using a CMOS UWB radar transceiver. In *New Circuits and Systems Conference (NEWCAS), 2016.*

[25] Zhicheng Yang, Parth H Pathak, Jianli Pan, Mo Sha, and Prasant Mohapatra. 2018. Sense and Deploy: Blockage-aware Deployment of Reliable 60 GHz mmWave WLANs. In *IEEE MASS 2018.* IEEE.

[26] Zhicheng Yang, Parth H Pathak, Yunze Zeng, Xixi Liran, and Prasant Mohapatra. 2017. Vital sign and sleep monitoring using millimeter wave. *ACM Transactions on Sensor Networks (TOSN)* 13, 2 (2017), 14.

[27] Zhicheng Yang, Parth H Pathak, Yunze Zeng, and Prasant Mohapatra. 2015. Sensor-assisted codebook-based beamforming for mobility management in 60 ghz wlans. In *IEEE MASS 2015.* IEEE, 333–341.

[28] Thomas Zwick, Werner Wiesbeck, Jens Timmermann, and Grzegorz Adamiuk. 2013. *Ultra-wideband RF system engineering.* Cambridge University Press.